Using the MSC/Nastran Superelement Modal Method to Improve the Accuracy of Predictive Fatigue Loads of a Short and Long Arm Type Rear Suspension

Dr. Hong Zhu, Dr. John Dakin and Ray Pountney, Ford Motor Company Limitd
Basildon Essex SS16 6EE UK

Abstract

In the fiercely competitive world of today's automotive industry, Computer Aided Engineering (CAE) is playing a more and more important role in shortening the design cycle time, minimising costs and improving the product quality.

For vehicle engineering, an optimised design is to develop a light-weight, safe and durable system. A key aspect of the fatigue/durability process is to quantify the vehicle service loads in the early design phase. Within the constraints of the development time, cost and quality, the trend has been to reduce road measurement, to use more rig simulation, to increase CAE prototypes and to decrease hardware prototypes. The accuracy of the CAE durability process is mandated to achieve a robust design.

This investigation includes an application of the MSC/Nastran superelement modal method to improve the load accuracy of a short and long arm typed rear suspension. Also a comparison is made between the loads obtained using rigid body dynamics and those including MSC/Nastran flexible bodies and to quantify the influence of the elastic suspension components such as links and knuckles.

Rigid body dynamic simulation methods usually neglect the flexibility and the modal properties of the elastic components. An integration of the MSC/Nastran superelement modal method with the MDI/Adams rigid body dynamics method offers an effective tool to improve the quality of the prediction of dynamic fatigue loads in the new product development.

1. Introduction

Rigid body dynamic analysis is efficient, but it ignores any component elasticity and simplifies dynamics of the mechanical components. Finite element analysis includes the elastic deformation and more accurate dynamic/inertia effects of the mechanical components, but it is not efficient for complex systems undergoing large displacements.

A combination of the finite element analysis with the rigid body dynamic analysis provides an effective method to generate predictive fatigue loads.

2. Theoretical Background

Superelements - Brief Review

A mechanical system consists of several superelements.

A superelement is a component made up of many finite elements.

A superelement is composed of interior Degrees Of Freedom (DOFs) and boundary DOFs.

The forces at all interior DOFs are set equal to zero. The boundary DOFs are located at the connection points of a superelement.

When rigid body representations of components undergo relatively large elastic deformations, they should be replaced with flexible bodies by means of the Nastran superelement.

The Modal Method

The physical displacements are transformed to modal displacements:

$$u(t)=\Sigma[\phi_i]\, q_i(t) \qquad (\, i=1, \text{Number of DOFs}) \qquad (1)$$

where:

$u(t)$ = physical displacement

$[\phi_i]$ = i-th mode shape

$q_i(t)$ = i-th modal displacement

Usually, the number of modes are significantly smaller than the number of physical degrees of freedom.

It is not practical and also not necessary to select the full set of free-free normal modes.

It is observed that the excitation frequency of the applied load is under a cut-off frequency determined by measurement sample rate and filtering in terms of experimental data. Therefore, the significant dynamic response can be enveloped by a set of finite modes, the response of the modes higher than the cut-off frequency will be quasi-static.

The $[\phi_i]$ may be partitioned into two sets of modes,

$$[\phi_i] \Rightarrow [\phi_n \quad \phi_s] \qquad (2)$$

where:

$[\phi_n]$ = normal mode shape (number of selective modes)

$[\phi_s]$ = static mode shape (number of interface DOFs)

Solve the eigenvalue problem using finite elements,

$\{[K] - \omega^2 [M]\}[\phi_n] = 0$ (3)

where:

ω^2 = eigenvalue

$$[K] = \begin{bmatrix} K^{BB} & K^{BI} \\ K^{IB} & K^{II} \end{bmatrix}$$ stiffness matrix

$$[M] = \begin{bmatrix} M^{BB} & M^{BI} \\ M^{IB} & M^{II} \end{bmatrix}$$ mass matrix

I = internal DOFs

B = boundary DOFs

Solve the static problem using finite elements,

$[K]\{u_s\} = \{F_t\}$ (4)

where:

$\{u_s\}$ = static displacement vector

$\{F_t\}$ = truncation force vector equivalent to applied force minus modally represented force

(for convenience, unit force can be applied to each the boundary DOFs successively with all other boundary DOFs fixed)

Form

$[K^*] = \{u_s\}^T [K] \{u_s\}$

$[M^*] = \{u_s\}^T [M] \{u_s\}$

Solve the pseudo eigenvalue problem using finite elements

$\{[K^*] - \omega^{*2} [M^*]\}[\phi^*_s] = 0$ (5)

The static mode shape is calculated,

$[\phi_s] = \{u_s\} [\phi^*_s]$ (6)

Finally, the mode set $[\phi_i] \Rightarrow [\phi_n \quad \phi_s]$ are orthonomalised and imported to the following coupling dynamic equation in Adams:

$$M\xi'' + M'\xi' - \tfrac{1}{2}[\partial M/\partial\xi\ \xi']^T \xi' + K\xi + f_g + D\xi' + [\partial\psi/\partial\xi]^T \lambda = Q \qquad (7)$$

where:

ξ, ξ', ξ'' = the flex body generalised co-ordinates and time derivatives

M, M' = the flex body mass matrix and its derivative

$\partial M/\partial\xi$ = partial derivative of M wrt generalised co-ordinates

K = the generalised stiffness matrix

f_g = the generalised gravitational force

D = the damping matrix

ψ = the constraint equations

λ = the Lagrange multipliers for the constraints

Q = vector of applied forces

Note that M matrix is a function of mode shapes. Detail of the various inertia invariants are available in the Adams/Flex Primer [1].

3. Nastran Superelement Models

3.1 Nastran Superelement Job Control

Nastran superelement normal mode solution is employed to extract modal information.

The difference of this analysis from the rountine superelement run is as follows:

1) User needs to include DMAP alter_N70 to write out the Nastran punch file with correct information to completely define a flexible body in Adams.
2) ECHO=PUNCH, SORT is required for Adams.
3) User must define connection points, that is hard points which represent location of constraints or loads in the mechanical system. The key statement is CSUPEXT.
4) User must define the number of modes. Key statements are SPOINT and SEQSET1.
5) User needs to make sure the co-ordinates of connection nodes of the Nastran superelement model are as same as those of connection marks of the Adams flexible body model.

The Nastran superelement example for a rear suspension front link is listed in Appendix A.

Two superelements, front link and knuckle, are created**.** Their information is as follows:

3.2 Superelement Front Link:

520 elements mainly CQUAD4.
492 Nodes
2 connection points
20 normal modes
12 static modes

3.3 Superelement Knuckle:

11543 elements mainly CQUAD4.
7978 Nodes
6 connection points
40 normal modes
36 static modes

It is obvious that the modal co-ordinates are much smaller than the physical co-ordinates.

The number of nodes does not directly affect the performance of the simulation. It is the number of modes and the number of connection points that impact simulation speed.

However, the number of nodes does affect the performance of the graphical pre- and post-processing.

3.4 Interface between Nastran and Adams

The Nastran punch file is translated to Adams modal neutral file by means of pch2mnf translator.

4. Adams Models

A short and long arm type rear suspension (SLA) is modelled using Adams and Adams/Flex.

The Adams rigid body model and the Adams flexible body of the suspension are shown in Fig.1 and 2. There are four flexible bodies in Fig.2, i.e., two front links and two knuckles on both the left and right hand side. The finite element models of the front link and the knuckle are shown in Fig.3.

The Adams flexible bodies are created by importing the modal neutral files.

For this application, modal neutral files, flink.mnf and knuckle.mnf, are imported to Adams.

It should be noted that the flexible bodies cannot be directly joined to each other, and also cannot be connected to bushes straight away (a current Adams limitation). The massless dummy parts and fixed joints are used at these positions.

The applied loads are 6 dimensional load time histories at each wheel centre.

The load time histories are measured loads at the vehicle proving ground via wheel force transducers. The event description for the complete durability route of 150k miles are tabulated in Table 1.

The constraints are applied to the vehicle body side of the bushes between the body to sub-frame.

5. Result and Analysis

The modal frequency sets of the front link and the knuckle are presented in tables 2 and 3.

In tables 2 and 3, the frequencies of normal modes are listed in Column 2 , and the frequencies of normal modes and static modes are included in Column 3. The frequencies are orthonomalised. It is seen that the frequency set of normal modes after orthonomalisation is very accurate in comparison with those from finite element calculation.

The modes higher than the maximum normal modes are static modes, but some static modes can be mixed with the normal modes. In other words, although the number of the modes including the normal modes and static modes is certain in an analysis, the sequence of the modes depends on the number of the retained normal modes and modal orthonomalisation.

It is not guaranteed that the static modes will always follow the normal modes.

Fig.4 shows the hard point description of the SLA rear suspension.

The tables 4 and 5 shows the comparison of rear suspension left and right peaks global loads from different sources. In tables 4 and 5, the major loads are highlighted by an asterisk. Note that in tables 4 and 5, f62 and f9 are calculated for the measured load set, whereas, f9 are measured for the calculated loads. The calculated loads are generally correlated with the measured loads with exception of the moments at pt9.

The moments at pt9 need to be investigated further.

The trend is that the loads using Adams flexible body model are closer to the measured loads than those using Adams rigid body model.
Since the loads on right hand side of the vehicle shows similar trend as those on left hand side, the subsequent analysis is concentrated on the left hand side. Five major component loads are chosen to make further analysis

The five component loads on the left hand side are:
f2xL=tie blade longitudinal load,
f7yL=upper link lateral load,
fdzL= damper vertical load,
f61yL=front low link lateral load,
f62yL=rear low arm lateral load.

The table 6 shows the comparison of the fatigue potential damage [2] from different sources for a complete suspension durability route.
The potential damage analysis is based on the uniaxial fatigue analysis using the local strain approach, as shown in Fig.5. Ideally fatigue life estimates obtained from finite element analysis being driven by experimental loads provides the best approach for durability assessment. However, due to time constraints it was decided to perform a potential damage analysis using the load time history data and the strain life curve only, as shown in Fig.6. Whilst this approach does not determine actual fatigue life it does allow an adequate assessment in terms of relative damageability from each of the different loading conditions.

Strain-Life Data are as follows:

Fatigue Strength Coefficient	sf'=600 N/mm2
Fatigue Strength Exponent	b=-0.087
Fatigue Ductile Coefficient	ef'=0.59
Fatigue Ductile Exponent	c=-0.58
Cyclic Strength coefficient	K'=600 N/mm2
Cyclic Strain Hardening Exponent	n'=0.15

For a comparison of two load time histories, the procedure is to perform potential damage analyses for a complete test route time history by factoring the first loads time history to produce an overall potential damage of 1 i.e. just meets the fatigue requirements. The load factor from the analysis of the first time history is used to perform the potential damage for the second load time history. The damage comparison can be made using a single dimensional load time history or different possible combinations of the three dimensional load time histories.
In the table 6, the most damaging event is highlighted by an asterisk. The exceptional case is highlighted by two asterisks. The values are still close in the exceptional case. By observation of the damage level of the major component load at the most damaged events such as event3, event5, event8, event12, event14 and event17, it is seen that the damage of loads from flexible body dynamics is closer to that of the measured loads than that from the rigid body dynamics in the majority of cases. The damage for the rigid and flex loads at each event is compared with that of baseline measured loads.

The Fig.7 to 11 show the five major load time histories on the event Chuckholes between the two Adams models. It is obvious that the loads for the rigid body model are higher than those for the coupled flexible body model. Since the fully instrumental measured loads are from a different data collection to that used for the dynamic analysis, they are not included in the time history plots.

The Fig.12 to 16 show the comparison of the level crossing counts for a defined suspension service life from different sources. The level crossing counting method counts the number of times a load time history passes through a set of user defined load levels. These plots of level crossing counts show that the predicted loads from the coupled flexible body model is more accurate than those from the rigid body model in correlation with the measured loads, this trend is more obvious towards the peak loads.

The modal representation in this investigation is linear, but the non-linear behaviour of the system can be represented by piecewise linear representation, i.e., by multiple flexible bodies appropriately jointed together (for example, twistbeam). This method can be extended to include the whole body structure.

6. Conclusions and Further Work

Loads calculated from rigid body dynamics are over-predicted as a result of neglecting component elasticity and modal characteristics.

Loads calculated from coupled rigid body and flexible body dynamics have a better correlation with the measured loads.

Nastran superelement modal method is practical and effective.

A further mode reduction is required to improve the simulation efficiency.

Table 1 - Proving Ground Events and Repetitions

Description	Event
Steering lock to Lock	01
Figure of Eight	02
Cobblestone Slalom	03
Chatter Bumps	04
Resonance Road part 1	05
Small Chuckholes	06
Railroad Crossing	07
Road 11 to Road 12 Intersection	08
Postel Road without Braking	09
Body Twist	10
Accel 5 Bumps	11
Large Chuckholes	12
Pt B, Road 11 to Postel Int.	13
Postel Road with Braking	14
Road 10	15
Kerb Island	16
Resonance Road Part 2	17
Jounce/Rebound Holes	18
Body Twist Slalom	19

Table 2 - Frequency List of the Front Link

Mode No	Frequency (Hz) No static	Frequency (Hz) With static	Mode No	Frequency (Hz) No static	Frequency (Hz) With static
1	0.028	0.000	17	5334.984	5364.151
2	0.031	0.000	18	6018.949	6023.984
3	0.031	0.012	19	6263.947	6296.056
4	0.034	0.022	20	6579.842	6620.197
5	0.038	0.026	21		6979.506
6	0.044	0.033	22		7255.833
7	553.056	553.086	23		7661.274
8	612.029	612.066	24		7791.368
9	1298.470	1299.424	25		8144.525
10	1674.102	1674.499	26		8479.880
11	2435.984	2438.890	27		9492.721
12	2969.268	2974.571	28		9506.543
13	3675.608	3677.447	29		10026.844
14	3834.148	3834.660	30		10051.648
15	3847.922	3873.613	31		10363.393
16	5117.348	5118.166	32		11816.178

Table 3 - Frequency List of the Knuckle

Mode No	Frequency (Hz) No static	Frequency (Hz) With static	Mode No	Frequency (Hz) No static	Frequency (Hz) With static
1	0.043	0.038	39	2331.732	2345.218
2	0.053	0.050	40	2365.445	2389.919
3	0.060	0.057	41		2439.346
4	0.061	0.057	42		2521.459
5	0.063	0.061	43		2627.365
6	0.064	0.062	44		2648.903
7	26.667	26.667	45		2755.647
8	108.745	108.746	46		2836.148
9	175.988	175.994	47		2903.100
10	315.848	315.857	48		3006.180
11	356.495	356.561	49		3033.273
12	435.888	436.133	50		3070.553
13	579.030	579.150	51		3093.723
14	652.709	652.921	52		3143.503
15	730.758	733.626	53		3216.347
16	892.340	893.332	54		3334.793
17	964.093	965.345	55		3392.889
18	991.984	993.091	56		3503.977
19	1045.222	1048.207	57		3543.026
20	1049.595	1053.317	58		3942.539
21	1189.511	1194.276	59		4128.202
22	1316.642	1321.488	60		4256.539
23	1374.577	1377.332	61		4502.855
24	1426.021	1427.682	62		4691.050
25	1517.957	1525.410	63		5060.996
26	1648.670	1657.166	64		5120.369
27	1668.502	1670.291	65		5369.120
28	1683.609	1709.386	66		5807.898
29	1726.907	1743.234	67		6209.088
30	1857.208	1866.092	68		6279.089
31	1885.772	1899.696	69		6636.637
32	1931.682	1957.551	70		6900.622
33	2013.771	2034.655	71		7862.280
34	2101.217	2136.289	72		8255.050
35	2163.584	2184.337	73		9633.708
36	2173.802	2197.519	74		11184.644
37	2214.978	2243.235	75		13965.901
38	2284.947	2325.227	76		45180.678

Table 4 - Comparison of Rear Suspension Left Knuckle Peak Loads

Maximum Loads on the Left Knuckle

	f2xL_g_max (N)	f2yL_g_max (N)	f2zL_g_max (N)	f7xL_g_max (N)	f7yL_g_max (N)	f7zL_g_max (N)
measured	5140*	551	970	317	1910*	2665
rigid	14667*	455	2110	478	8159*	2968
flex	6568*	257	1276	647	2224*	3009

	f9xL_g_max (N)	f9yL_g_max (N)	f9zL_g_max (N)	m9xL_g_max (Nmm)	m9yL_g_max (Nmm)	m9zL_g_max (Nmm)
measured	13375	5575	8732	1140154	34136	1213221
rigid	9244	5293	13156	1441206	345380	439780
flex	9243	5293	13156	1441206	345380	439780

	fdxL_g_max (N)	fdyL_g_max (N)	fdzL_g_max (N)	f61xL_g_max (N)	f61yL_g_max (N)	f61zL_g_max (N)
measured	1516	3282	7417*	507	9681*	1995
rigid	947	4962	8068*	895	16793*	2801
flex	906	4263	7226*	630	13268*	2798

	f62xL_g_max (N)	f62yL_g_max (N)	f62zL_g_max (N)
measured	334	4831*	1029
rigid	940	6125*	1000
flex	878	6289*	1165

Minimum Loads on the Left Knuckle

	f2xL_g_min (N)	f2yL_g_min (N)	f2zL_g_min (N)	f7xL_g_min (N)	f7yL_g_min (N)	f7zL_g_min (N)
measured	-12481*	-475	-832	-688	-8782*	-887
rigid	-14926*	-411	-2934	-817	-10187*	-1123
flex	-15629*	-325	-2571	-835	-8180*	-1110

	f9xL_g_min (N)	f9yL_g_min (N)	f9zL_g_min (N)	m9xL_g_min (Nmm)	m9yL_g_min (Nmm)	m9zL_g_min (Nmm)
measured	-5969	-5321	-6035	-416220	-926631	-685434
rigid	-2399	-3983	-562	-975403	-221826	-460507
flex	-2399	-3983	-562	-975403	-221826	-460507

	fdxL_g_min (N)	fdyL_g_min (N)	fdzL_g_min (N)	f61xL_g_min (N)	f61yL_g_min (N)	f61zL_g_min (N)
measured	-2111	-2163	-3281*	-1688	-2933*	-1733
rigid	-3687	-1424	-2513*	-3546	-6779*	-2875
flex	-3066	-1368	-2432*	-3311	-3912*	-2873

	f62xL_g_min (N)	f62yL_g_min (N)	f62zL_g_min (N)
measured	-380	-6648*	-6771
rigid	-872	-10495*	-2937
flex	-451	-5167*	-2911

Global Axes Description

- x-axis : positive vehicle backwards
- y-axis : positive vehicle left to right
- z-axis : positive vehicle upwards

Point Description on Knuckle (L=left : R=right)

- pt2 - tie blade
- pt7 - upper link
- pt9 - wheel centre
- ptd - damper
- pt61 - front lower link
- pt62 - rear lower arm

End of the Table 4

Table 5 - Comparison of Rear Suspension Right Knuckle Peak Loads

Maximum Loads on the Right Knuckle

	f2xR_g_max (N)	f2yR_g_max (N)	f2zR_g_max (N)	f7xR_g_max (N)	f7yR_g_max (N)	f7zR_g_max (N)
measured	4617*	92	679	259	8068*	2388
rigid	7728*	476	3958	389	10228*	2265
flex	6913*	351	1059	476	6558	2269

	f9xR_g_max (N)	f9yR_g_max (N)	f9zR_g_max (N)	m9xR_g_max (Nmm)	m9yR_g_max (Nmm)	m9zR_g_max (Nmm)
measured	11113	4186	9559	317657	107709	700031
rigid	8258	4117	12053	1049131	215801	463169
flex	8258	4117	12053	1049131	215801	463169

	fdxR_g_max (N)	fdyR_g_max (N)	fdzR_g_max (N)	f61xR_g_max (N)	f61yR_g_max (N)	f61zR_g_max (N)
measured	1450	2066	3507*	536	2620*	1797
rigid	990	1465	7426*	853	4562*	3102
flex	859	1260	6632*	515	3410*	2754

	f62xR_g_max (N)	f62yR_g_max (N)	f62zR_g_max (N)
measured	335	6473*	474
rigid	847	7168*	688
flex	344	4658*	736

Minimum Loads on the Right Knuckle

	f2xR_g_min (N)	f2yR_g_min (N)	f2zR_g_min (N)	f7xR_g_min (N)	f7yR_g_min (N)	f7zR_g_min (N)
measured	-10311*	-1230	-1208	-608	-1353*	-867
rigid	-14344*	-259	-4482	-584	-7623*	-1249
flex	-14254*	-142	-2164	-595	-2227*	-1268

	f9xR_g_min (N)	f9yR_g_min (N)	f9zR_g_min (N)	m9xR_g_min (Nmm)	m9yR_g_min (Nmm)	m9zR_g_min (Nmm)
measured	-4419	-6143	-2714	-1309271	-828498	-1666876
rigid	-3279	-4530	-568	-1265392	-404858	-459790
flex	-3279	-4530	-568	-1265392	-404858	-459790

	fdxR_g_min (N)	fdyR_g_min (N)	fdzR_g_min (N)	f61xR_g_min (N)	f61yR_g_min (N)	f61zR_g_min (N)
measured	-1300	-1851	-3055*	-1774	-9727*	-1770
rigid	-3362	-4498	-2276*	-4051	-14648*	-2226
flex	-3020	-3986	-2010*	-3434	-12952*	-2180

	f62xR_g_min (N)	f62yR_g_min (N)	f62zR_g_min (N)
measured	-429	-4479*	-7241
rigid	-488	-6458*	-2891
flex	-415	-5337*	-2885

Global Axes Description

x-axis : positive vehicle backwards
y-axis : positive vehicle left to right
z-axis : positive vehicle upwards

Point Description on Knuckle (L=left : R=right)

pt2 - tie blade
pt7 - upper link
pt9 - wheel centre
ptd - damper
pt61 - front lower link
pt62 - rear lower arm

End of the Table 5

Table 6 - Comparison of the Potential Damage from Different Sources

f2xL - tie blade longitudinal loads

Event No.	Measured		Rigid		Flex	
	damage	percentage	damage	percentage	damage	percentage
event 1	0.000	0.000	0.000	0.000	0.000	0.000
event 2	0.000	0.000	0.000	0.000	0.000	0.000
event 3**	0.692	65.832	7.248	44.139	8.271	50.117
event 4	0.000	0.041	0.975	5.940	0.856	5.187
event 5*	0.020	1.860	1.995	12.147	1.798	10.893
event 6	0.123	11.669	0.205	1.250	0.252	1.526
event 7	0.002	0.169	0.111	0.674	0.115	0.695
event 8*	0.000	0.002	0.035	0.211	0.043	0.259
event 9	0.000	0.000	0.000	0.000	0.000	0.000
event 10	0.000	0.029	0.009	0.056	0.010	0.063
event 11	0.000	0.031	0.069	0.421	0.091	0.550
event 12*	0.084	7.945	0.613	3.731	0.637	3.859
event 13	0.000	0.000	0.007	0.044	0.009	0.052
event 14*	0.002	0.218	0.165	1.002	0.159	0.965
event 15	0.000	0.000	0.000	0.001	0.000	0.001
event 16	0.000	0.017	0.013	0.079	0.015	0.089
event 17*	0.120	11.394	4.927	30.004	4.194	25.415
event 18	0.008	0.791	0.014	0.086	0.020	0.124
event 19	0.000	0.000	0.035	0.215	0.034	0.204
total dam	1.051	100.000	16.421	100.000	16.504	100.000

f7yL - upper link lateral loads

Event No.	Measured		Rigid		Flex	
	damage	percentage	damage	percentage	damage	percentage
event 1	0.000	0.000	0.000	0.015	0.001	0.061
event 2	0.000	0.033	0.002	0.065	0.002	0.077
event 3*	0.206	18.950	0.456	17.225	0.274	12.105
event 4	0.045	4.139	0.169	6.385	0.160	7.087
event 5*	0.076	7.024	0.356	13.454	0.254	11.224
event 6	0.056	5.131	0.049	1.832	0.068	3.026
event 7	0.022	2.061	0.045	1.714	0.048	2.111
event 8*	0.123	11.303	0.229	8.648	0.197	8.707
event 9	0.004	0.343	0.000	0.005	0.000	0.007
event 10	0.001	0.076	0.003	0.096	0.003	0.113
event 11	0.003	0.297	0.014	0.510	0.015	0.647
event 12*	0.184	16.900	0.128	4.833	0.162	7.183
event 13	0.021	1.918	0.041	1.548	0.038	1.676
event 14*	0.008	0.743	0.018	0.697	0.019	0.822
event 15	0.000	0.000	0.002	0.068	0.000	0.009
event 16	0.005	0.451	0.008	0.295	0.005	0.217
event 17*	0.274	25.184	0.956	36.072	0.884	39.109
event 18	0.007	0.644	0.014	0.510	0.013	0.592
event 19	0.052	4.804	0.160	6.029	0.118	5.227
total dam	1.087	100.000	2.649	100.000	2.260	100.000

fdzL - damper vertical loads

Event No.	Measured		Rigid		Flex	
	damage	percentage	damage	percentage	damage	percentage
event 1	0.000	0.000	0.000	0.000	0.000	0.000
event 2	0.000	0.000	0.000	0.000	0.000	0.000
event 3*	0.136	12.492	0.327	7.137	0.210	6.445
event 4	0.070	6.431	0.519	11.328	0.346	10.636
event 5*	0.252	23.073	0.868	18.968	0.608	18.709
event 6	0.019	1.709	0.090	1.963	0.077	2.372
event 7	0.010	0.899	0.083	1.823	0.063	1.935
event 8*	0.014	1.320	0.070	1.522	0.054	1.655
event 9	0.000	0.006	0.000	0.001	0.000	0.000
event 10	0.000	0.033	0.001	0.017	0.001	0.024
event 11	0.012	1.121	0.030	0.650	0.025	0.757
event 12*	0.064	5.899	0.343	7.490	0.276	8.477
event 13	0.003	0.289	0.015	0.332	0.012	0.383
event 14*	0.012	1.060	0.056	1.228	0.038	1.155
event 15	0.000	0.002	0.000	0.001	0.000	0.000
event 16	0.008	0.756	0.009	0.186	0.006	0.192
event 17*	0.481	44.156	2.122	46.348	1.497	46.048
event 18	0.007	0.669	0.007	0.148	0.005	0.164
event 19	0.001	0.086	0.039	0.860	0.034	1.046
total dam	1.090	100.000	4.578	100.000	3.251	100.000

f61yL - front low link lateral loads

Event No.	Measured		Rigid		Flex	
	damage	percentage	damage	percentage	damage	percentage
event 1	0.000	0.000	0.000	0.001	0.000	0.005
event 2	0.001	0.054	0.003	0.052	0.003	0.069
event 3*	0.401	39.165	1.454	24.087	1.029	24.077
event 4	0.023	2.213	0.444	7.353	0.258	6.041
event 5*	0.127	12.374	0.920	15.240	0.625	14.629
event 6	0.031	3.026	0.086	1.432	0.078	1.834
event 7	0.011	1.114	0.062	1.021	0.053	1.239
event 8*	0.049	4.766	0.208	3.446	0.191	4.458
event 9	0.001	0.096	0.000	0.001	0.000	0.001
event 10	0.003	0.248	0.005	0.082	0.004	0.094
event 11	0.010	0.939	0.042	0.693	0.038	0.897
event 12*	0.042	4.141	0.271	4.497	0.225	5.254
event 13	0.009	0.866	0.038	0.632	0.037	0.873
event 14*	0.007	0.679	0.057	0.949	0.038	0.894
event 15	0.000	0.000	0.000	0.003	0.000	0.002
event 16	0.002	0.205	0.008	0.130	0.005	0.119
event 17*	0.290	28.340	2.299	38.096	1.573	36.791
event 18	0.004	0.422	0.010	0.173	0.010	0.225
event 19	0.014	1.350	0.127	2.109	0.107	2.499
total dam	1.024	100.000	6.036	100.000	4.275	100.000

```
f62yL - rear low link lateral loads
-----------------------------------
```

Event No.	Measured		Rigid		Flex	
	damage	percentage	damage	percentage	damage	percentage
event 1	0.000	0.000	0.000	0.000	0.000	0.000
event 2	0.003	0.292	0.000	0.015	0.000	0.021
event 3*	0.733	67.664	1.598	64.031	1.120	71.239
event 4	0.005	0.418	0.113	4.533	0.013	0.805
event 5*	0.007	0.628	0.104	4.160	0.013	0.803
event 6	0.095	8.739	0.104	4.158	0.118	7.526
event 7	0.003	0.242	0.008	0.306	0.004	0.224
event 8*	0.083	7.666	0.057	2.271	0.042	2.676
event 9	0.001	0.047	0.000	0.000	0.000	0.000
event 10	0.003	0.262	0.004	0.168	0.004	0.275
event 11	0.000	0.005	0.001	0.031	0.001	0.039
event 12*	0.091	8.432	0.139	5.587	0.138	8.810
event 13	0.013	1.157	0.009	0.342	0.007	0.473
event 14*	0.003	0.308	0.013	0.511	0.008	0.532
event 15	0.000	0.000	0.000	0.002	0.000	0.000
event 16	0.001	0.124	0.002	0.064	0.002	0.096
event 17*	0.028	2.580	0.296	11.877	0.062	3.965
event 18	0.008	0.775	0.004	0.156	0.004	0.241
event 19	0.007	0.661	0.045	1.789	0.036	2.275
total dam	1.083	100.000	2.496	100.000	1.572	100.000

End of the Table 6

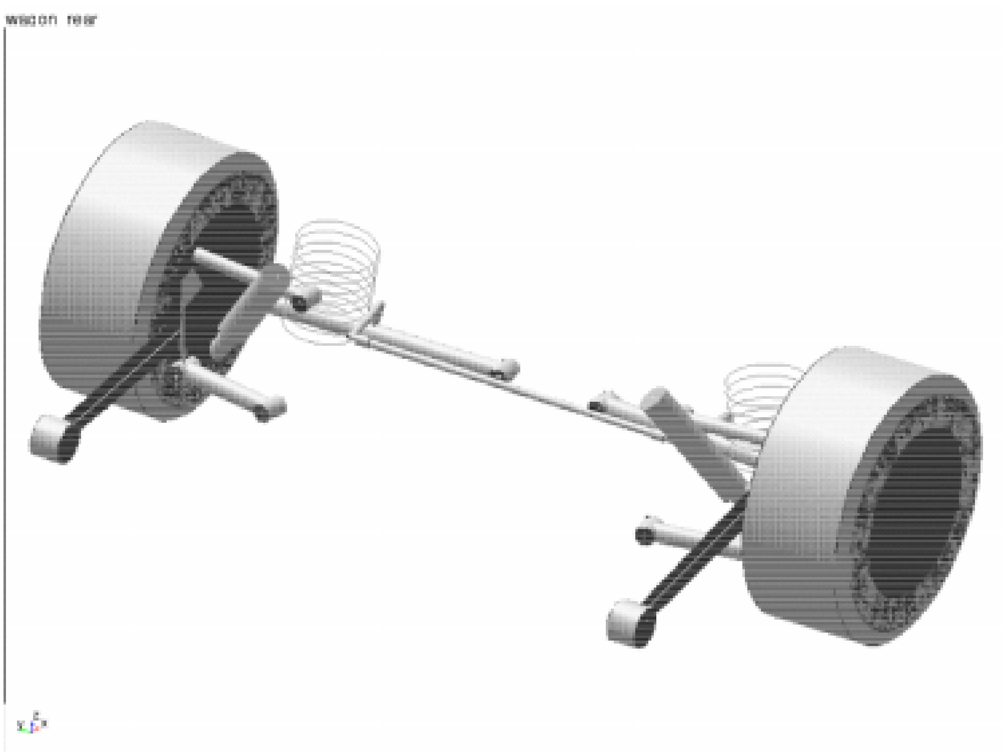

Fig.1 - Rigid Body Dynamic Model of Rear Suspension

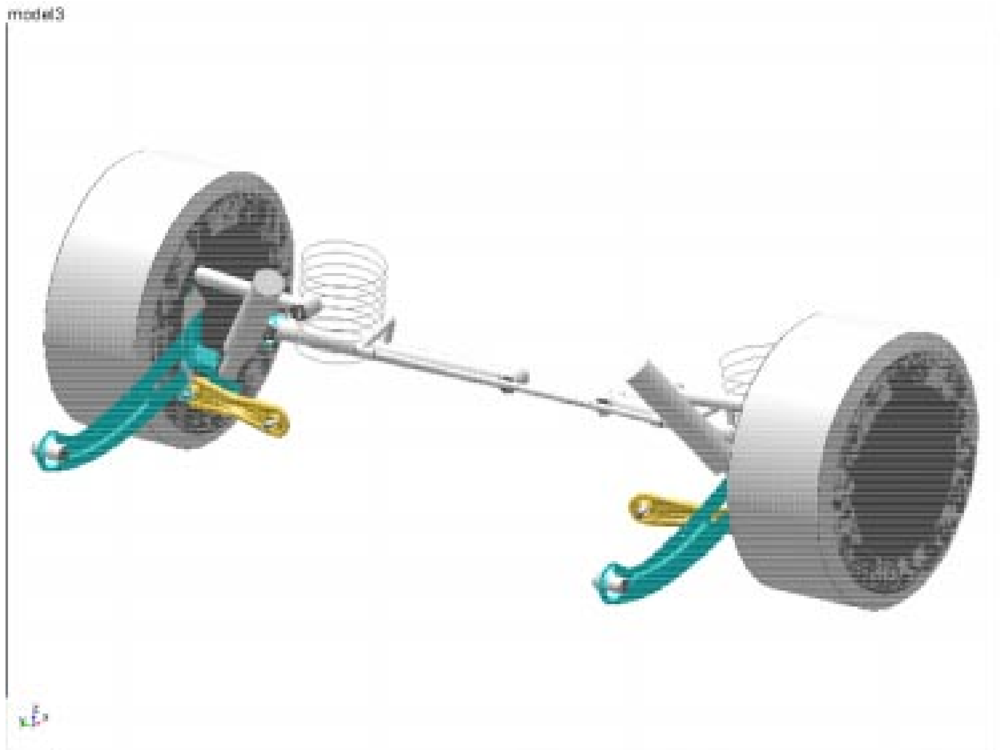

Fig.2 - Coupled Rigid Body and Flexible Body Dynamic Model of Rear Suspension

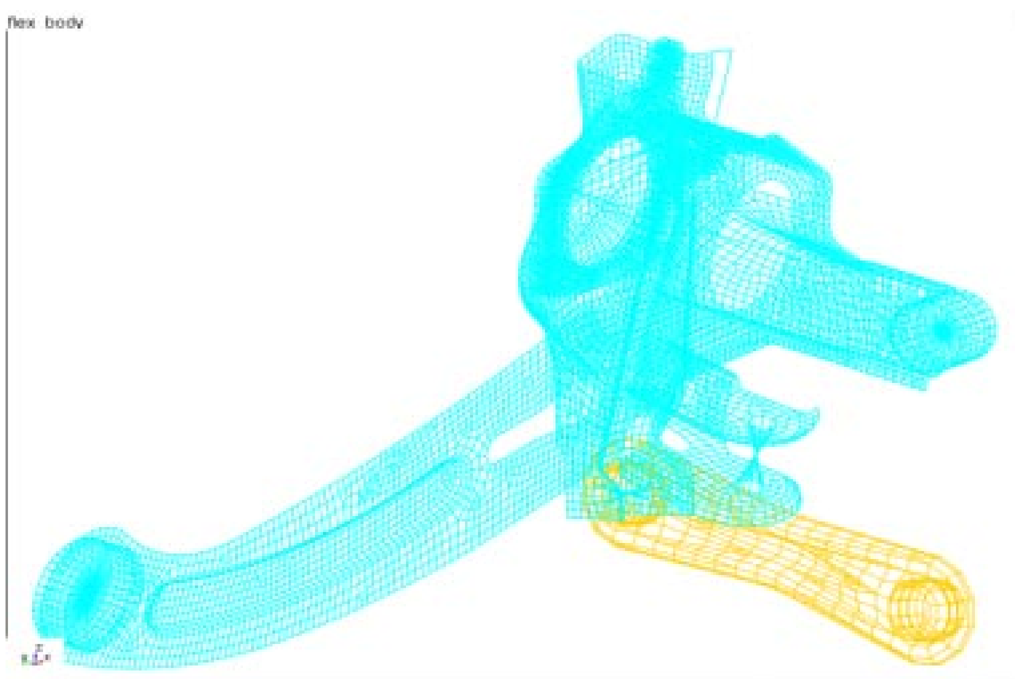

Fig.3 - Finite Element Model of the Front Link and the Knuckle

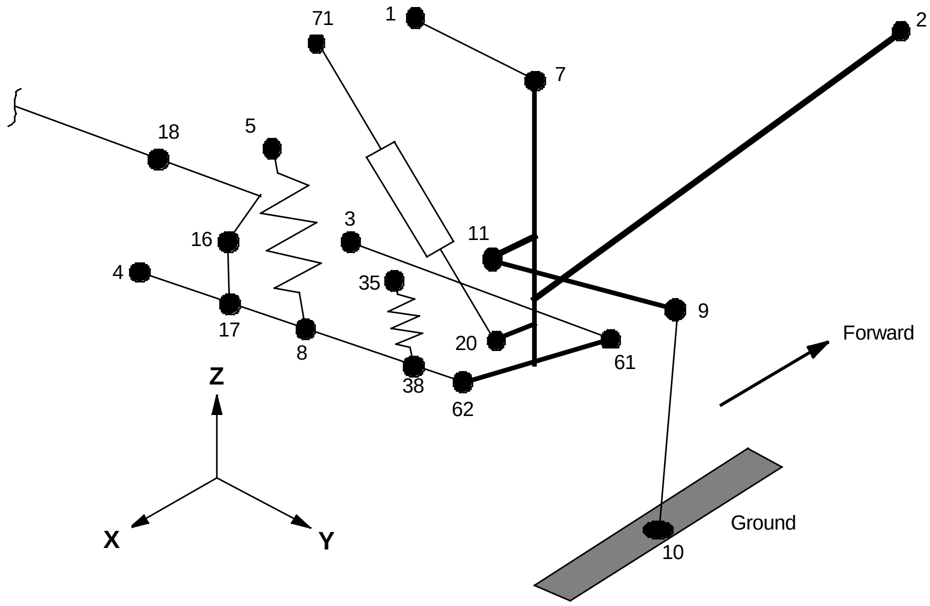

Location	Point No.
Upper link / crossmember	1
Tie bar / Body	2
Front lower link / Crossmember	3
Rear lower link / Crossmember	4
Spring / Crossmember	5
Upper link / Knuckle	7
Spring / Rear lower link	8
Wheel Centre	9
Tyre / Ground Contact	10
Point on axle centre line	11
A-Roll Bar Link / Bar	16
A-Roll Bar Link / Lower arm	17
Anti-roll bar / Crossmember	18
Damper / knuckle	20
B stop, S Assist / Crossmember	35
B stop, S Assist / Rear lower link	38
Front lower link / Knuckle	61
Rear lower link / Knuckle	62
Damper / Crossmember	71

Fig.4 - Hard Point Description of the SLA Rear Suspension

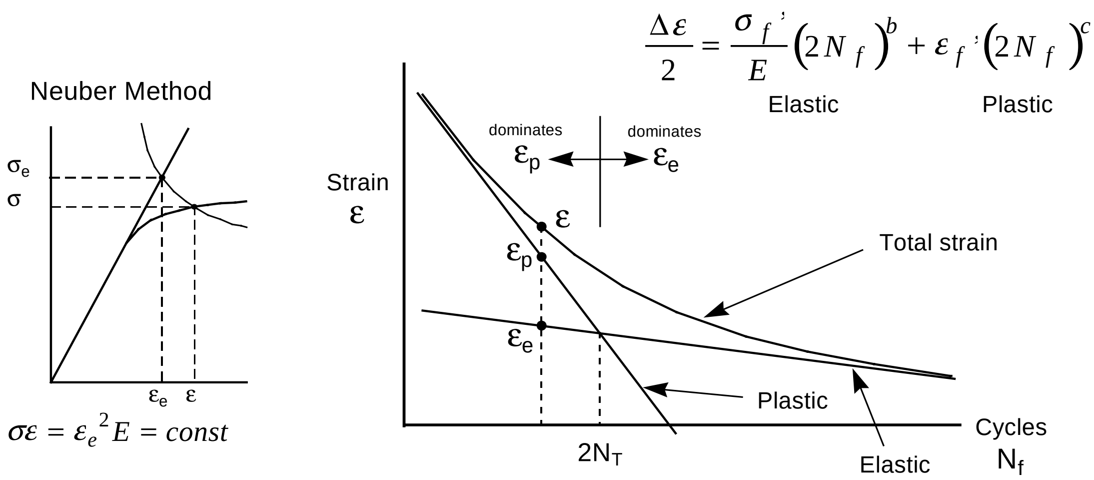

Fig.5 - Strain Life Approach

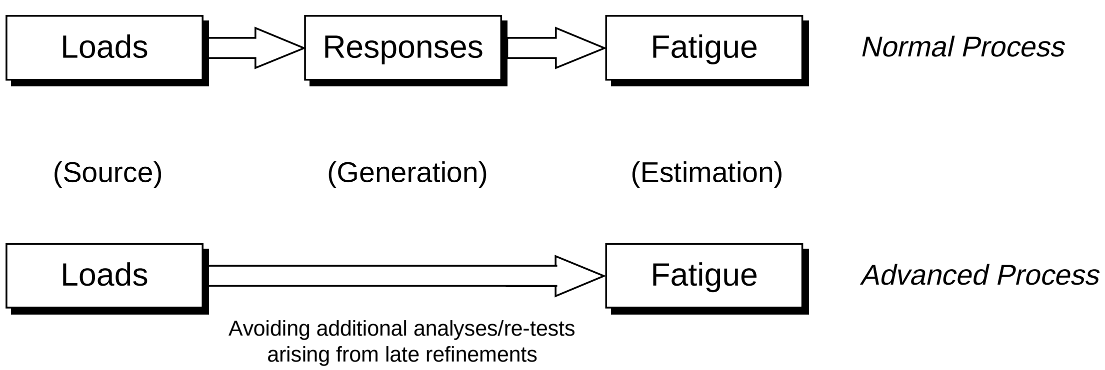

Fig.6 - Potential Damage Process

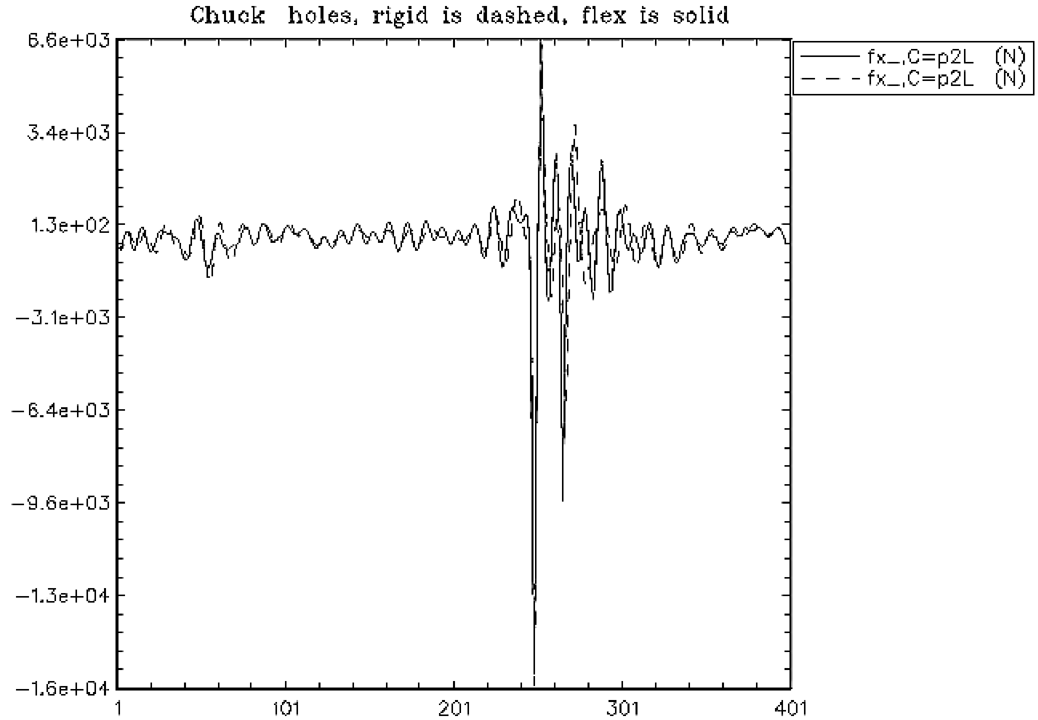

Fig.7 - Event Chuckholes - Tie Blade Longitudinal Loads, Adams Dynamics

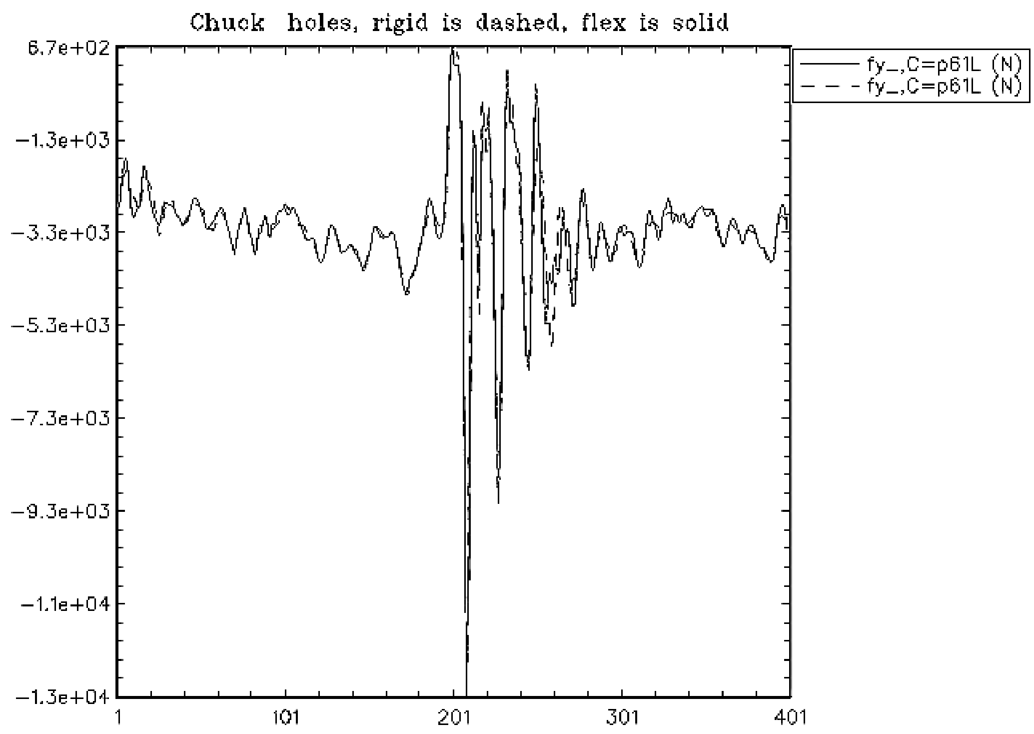

Fig.8 - Event Chuckholes - Front Low Link Lateral Loads, Adams Dynamics

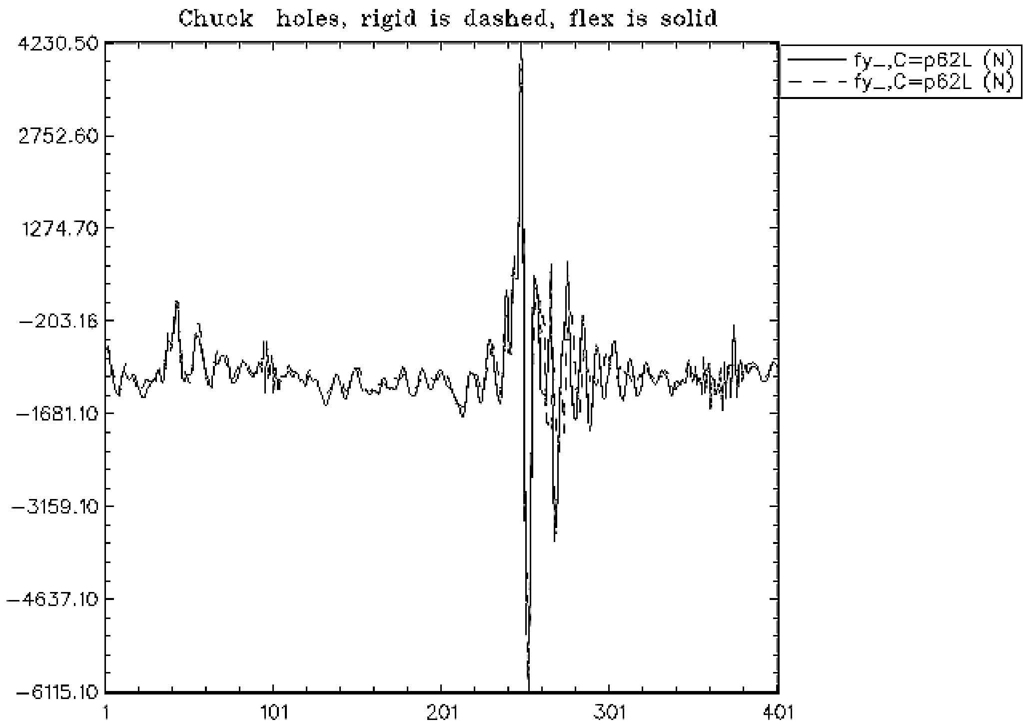

Fig.9- Event Chuckholes - Rear Low Arm Lateral Loads, Adams Dynamics

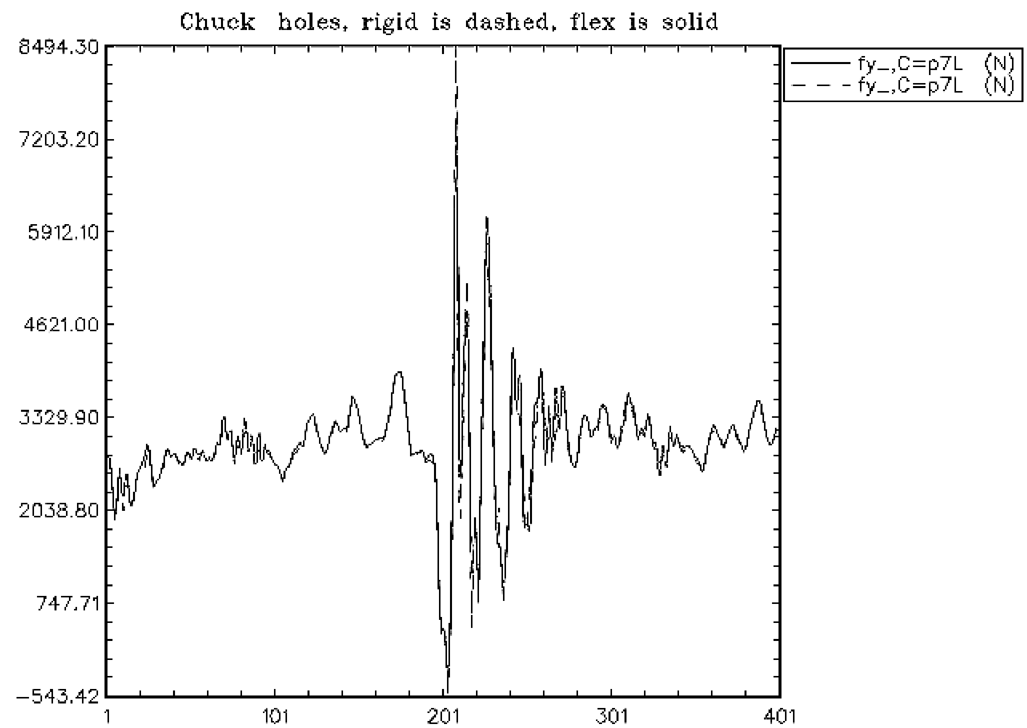

Fig.10 - Event Chuckholes - Upper Link Lateral Loads, Adams Dynamics

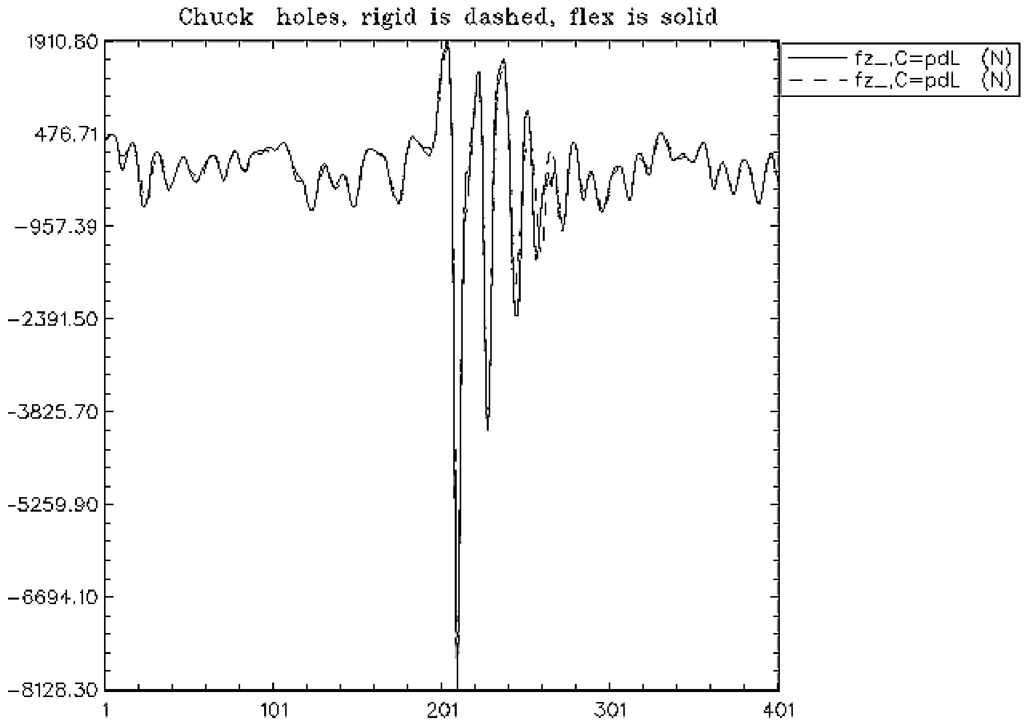

Fig.11 - Event Chuckholes - Damper Vertical Loads, Adams Dynamics

Tue Mar 16 13:27:40 1999

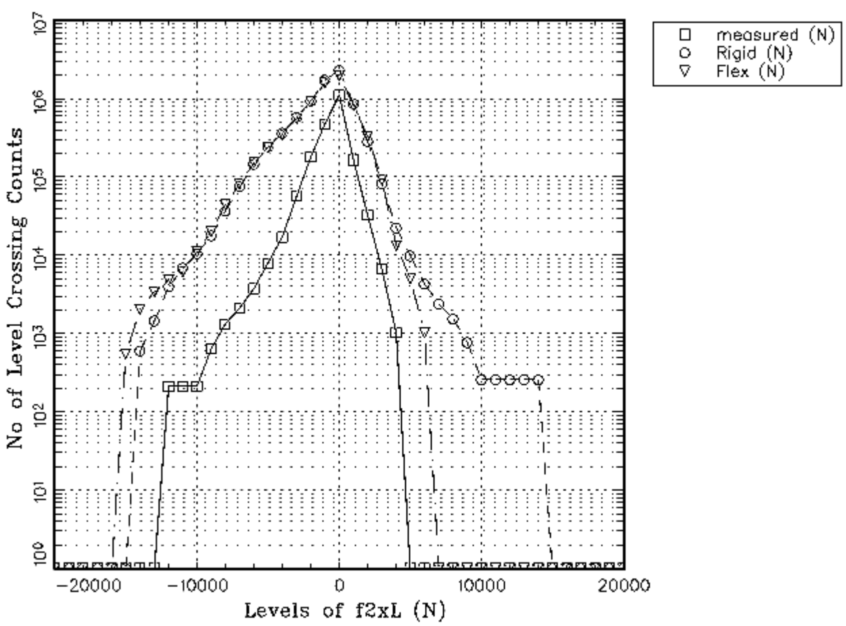

Fig.12 - Comparison of Level Crossing Counts of Tie Blade Longitudinal Loads

Tue Mar 16 13:34:31 1999

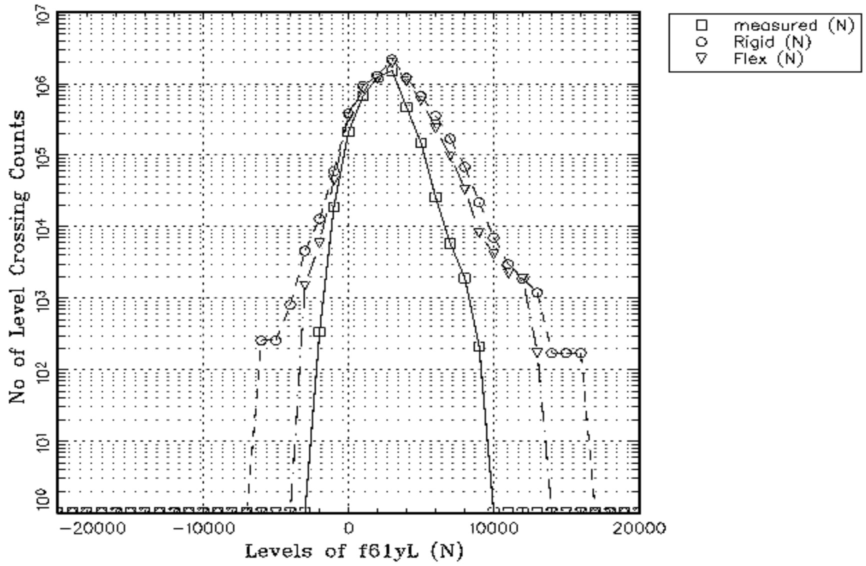

Fig.13 - Comparison of Level Crossing Counts of Front Low Link Lateral Loads

Tue Mar 16 15:12:50 1999

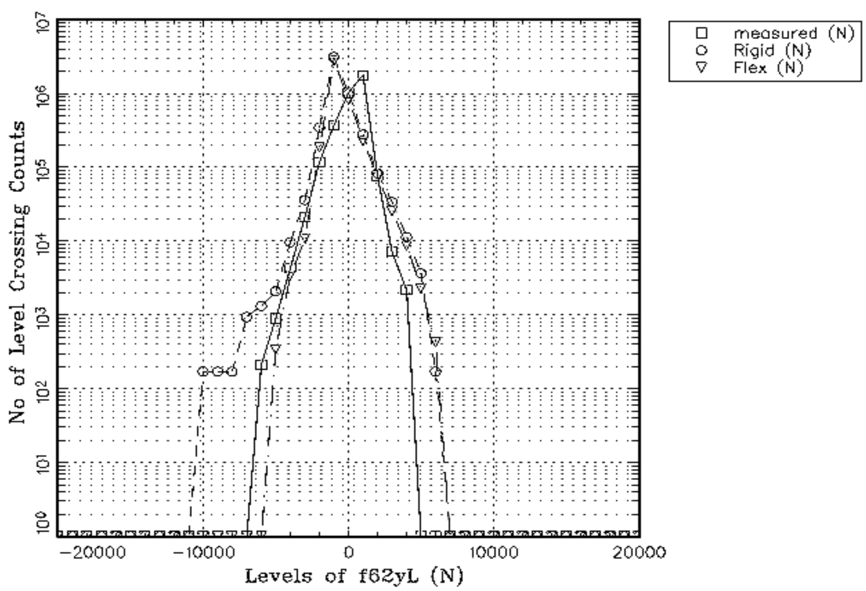

Fig.14 - Comparison of Level Crossing Counts of rear Low Arm Lateral Loads

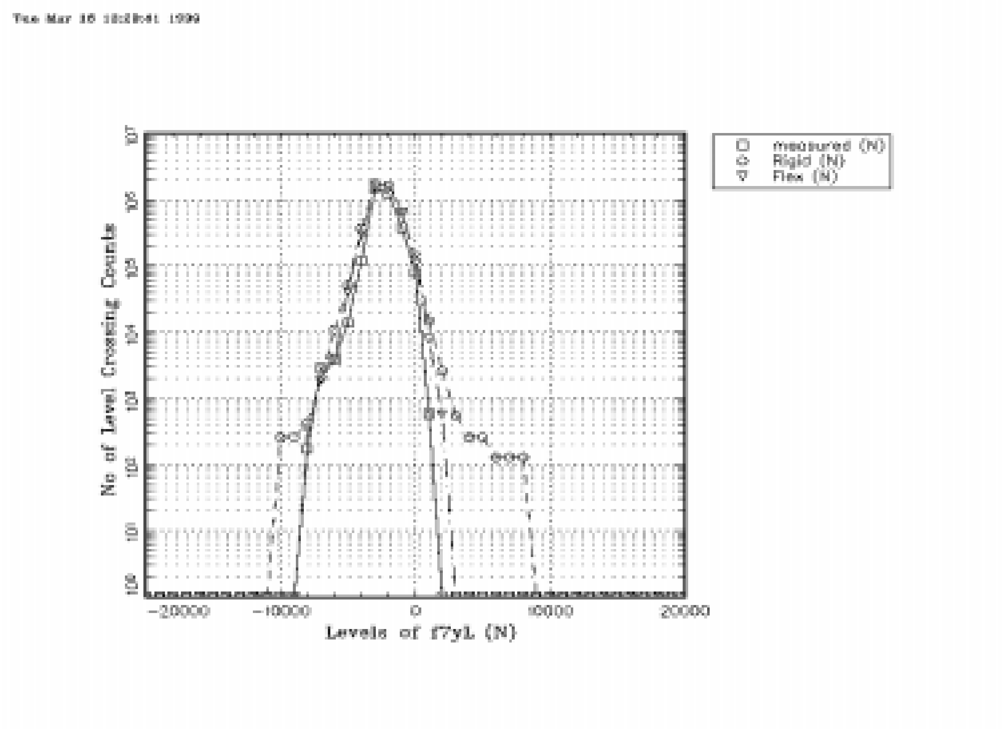

Fig.15 - Comparison of Level Crossing Counts of Upper Link Lateral Loads

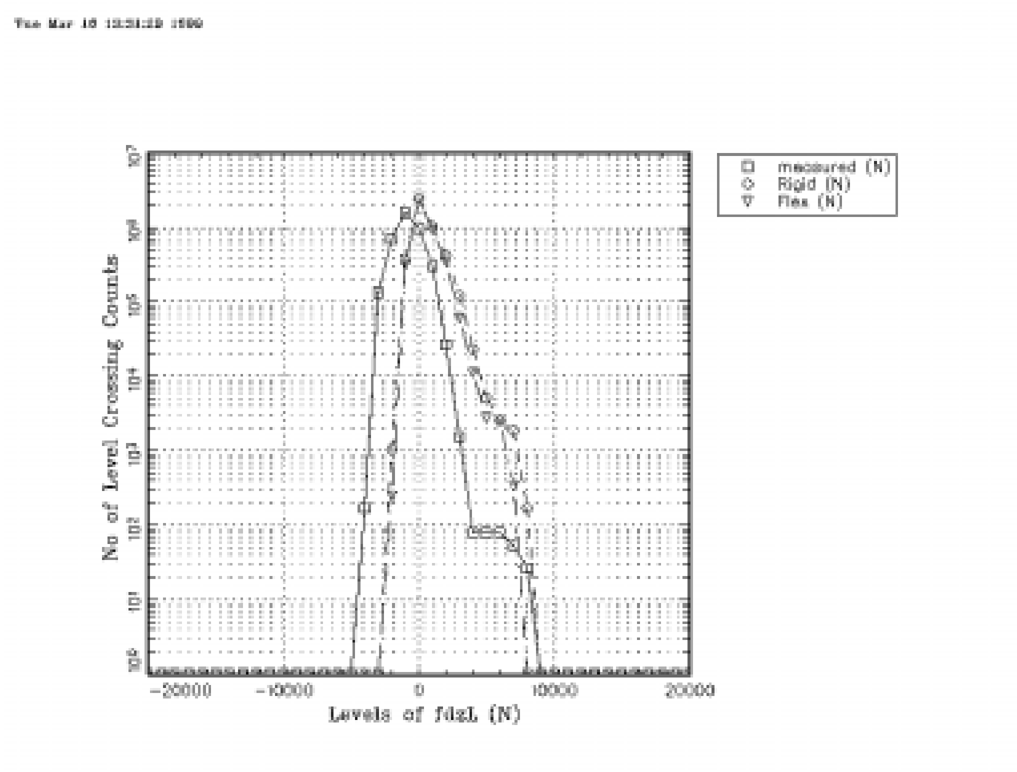

Fig.16 - Comparison of Level Crossing Counts of Damper Vertical Loads

Reference

1 .Adams/Flex V9.1 User's Guide, Mechanical Dynamics, Inc
2. MDE V2.3 User's Reference Manuals, MTS System Corporation